Multifunctional Biosensor Based on Localized Surface Plasmon Resonance for Monitoring Small Molecule–Protein Interaction

Joana Rafaela Lara Guerreiro,[§,†,‡] Maj Frederiksen,[§] Vladimir E. Bochenkov,[⊥,§] Victor De Freitas,[‡] Maria Goreti Ferreira Sales,[†] and Duncan Steward Sutherland[§,*]

[†]BioMark Sensor Research, Instituto Superior de Engenharia do Porto, 4200-072 Porto, Portugal, [‡]Departamento de Química, Centro de Investigação em Química, Faculdade de Ciências da Universidade do Porto, 4169-007 Porto, Portugal, [§]Interdisciplinary Nanoscience Center (iNANO), Aarhus University, DK-8000 Aarhus, Denmark, and [⊥]Department of Chemistry, Lomonosov Moscow State University, 119991 Moscow, Russia

ABSTRACT We report an optical sensor based on localized surface plasmon resonance (LSPR) to study small-molecule protein interaction combining high sensitivity refractive index sensing for quantitative binding information and subsequent conformation-sensitive plasmon-activated circular dichroism spectroscopy. The interaction of α-amylase and a small-size molecule (PGG, pentagalloyl glucose) was log concentration-dependent from 0.5 to 154 μM. *In situ* tests were additionally successfully applied to the analysis of real wine samples. These studies demonstrate that LSPR sensors to monitor small molecule–protein interactions in real time and *in situ*, which is a great advance within technological platforms for drug discovery.

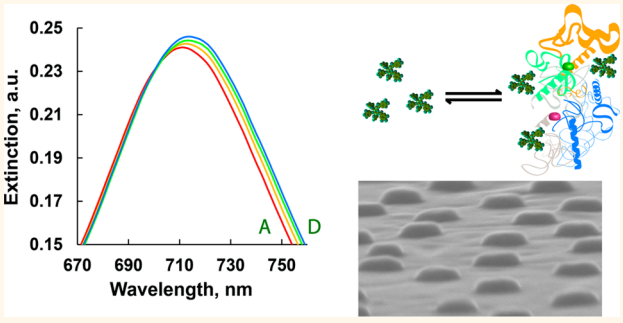

KEYWORDS: colloidal lithography · biosensing · localized surface plasmon resonance (LSPR) · small molecules · nanodisks · α-amylase

Small molecule interactions with proteins play a critical role in the regulation of a broad range of biological processes and cellular activities.[1,2] Identification and study of these interactions is central in the discovery and development of new pharmaceuticals and enables mechanistic understanding of both native cellular regulatory processes and drug molecule action. In the past few years a range of efforts were made to study the interaction of small molecules with proteins with a focus on, for example, target affinities[3] or differences in the stability of unbound *versus* small molecule-bound proteins[4] giving an enrichment of the understanding of biological processes.[5−8] There is a need to develop methods and tools that can be used to both quantitatively and mechanistically investigate this important and rich class of interactions.

Recently, several localized surface plasmon resonance (LSPR) sensors were reported for the detection of biomolecules, protein–protein interactions, surface binding events, antigen–antibody recognition[9] and biointeractions, due to their high sensitivity, good reproducibility, real-time responses and label-free detection.[10−15] LSPR's are oscillations of the conduction electrons at metal nanostructures (typically Au, Ag or Al or recently observed at graphene semimetals[16−18]) with highly confined oscillating electric fields that extend into the surroundings. These localization of the LSPR and the highly sensitive dependence of the resonance energy on refractive index mean that the adsorption of biomolecules causes the shift of the LSPR peak wavelength with larger RI changes giving higher signals.[19,20] This type of quantifiable but label-free detection is especially important in interaction studies ensuring that the interaction process is not affected by the presence of a label, mimicking the natural interaction and making the detection relatively easy to perform.[21,22] Therefore, LSPR sensing provides an interesting tool to

* Address correspondence to duncan@inano.au.dk.

Received for review April 8, 2014 and accepted July 8, 2014.

Published online July 08, 2014
10.1021/nn501962y

detect and explore the interaction of small molecules and proteins.

Besides the intrinsic complexity of small molecule–protein interactions they are often accompanied by conformational adaptations of the target protein, which are typically responsible for regulatory capacity in the biological system. Structural X-ray diffraction studies of crystallized proteins with small-molecule binding partners have been made, giving detailed pictures of binding pockets and static pictures of conformational states resulting from interaction,[23] while spectroscopies such as circular dichroism (CD)[24−27] and small-angle X-ray scattering (SAXS)[28−30] can show conformational changes in more native environments. These studies are used with high quality information to elaborate modes of action and ligand binding sites of drug candidates often in combination with *in silico* efforts.[31−34] Changes of protein conformation are common events in biological systems, however, deregulations may occur due to improper ligand binding or protein misfolding, leading to the appearance of diseases.[35] Therefore, the detection of conformational changes of proteins or enzymes promoted by molecular interactions could also provide valuable information regarding the prevention of diseases or keep track of molecules that provide information on diseases stage.[36,37] Alzheimer's, Parkinson's and Huntingston's diseases are examples of still nontreatable diseases, commonly characterized by adoption of abnormal conformations in oligomeric and fibril forms resulting from aggregation of proteins,[38] though recent works suggested polyphenols compounds as remarkable inhibitors of aggregation in amyloid diseases.[39] Approaches which could be used to combine quantitation of small molecule binding with information on conformational alteration in a screening format would have useful application both in the health area for drug candidate identification and study of disease molecular mechanisms as well as for the detection of biological agents in the environment,[40] in food safety[41,42] or in security applications,[43,44] while quantitative sensors could be applied for control in complex industrial processes. For instance, an important parameter to evaluate red wine quality is called astringency, which can be estimated by the binding affinity of polyphenols present in wine with salivary proteins.[45]

Here we present a multifunctional biosensor for the study of small molecule–protein interaction based on localized surface plasmon resonances which combines high sensitivity refractive index sensing giving quantitative binding information and conformation-sensitive plasmon-activated CD spectroscopy on the same sample from monolayers of proteins at nanostructures. As a model we used the most common enzyme/protein found in saliva, α-amylase (AMY) and a small molecule pentagalloyl glucose (PGG) a polyphenol which consist of a glucose molecule linked to five gallic acids.

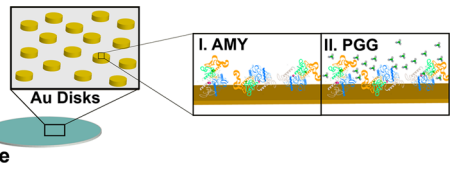

Figure 1. Scheme of the binding process, after AMY (I) and upon PGG binding (II).

Comparison of the experimental and simulated data by finite-difference time-domain (FDTD) simulations, allowed quantification of the amounts of PGG binding per AMY which were correlated to structural information from literature. Additionally, plasmonic nanostructures were used to probe changes in the chiral properties of the local dielectric environment giving *in situ* information on conformational alterations of adsorbed AMY upon interaction with PGG.

RESULTS AND DISCUSSION

LSPR Fabrication and AMY/PGG Interactions. AMY was selected due to its important role in both digestion and as a biological indicator for further disease diagnostics.[46,47] AMY is a glycoprotein of 53.5 kDa[48] that adopts an ellipsoid geometry formed from a polypeptide chain of 496 amino acids presenting an unusual high proportion (12.5%) of aromatic residues.[49] The presence of aromatic residues and the hydrophobic sites of the side chains of proteins seem to be important sites for binding of PGG.[50] Polyphenols with both high and low molecular weight can interact with AMY or other biological proteins, promoting beneficial effects on health,[51] affecting sensorial[52] properties or causing inhibition,[45] the general sensing scheme is shown in Figure 1.

The fabrication of Au nanodisks on a glass substrate was based on hole mask colloidal lithography,[53] allowing the creation of specific spots for AMY immobilization. The cylindrical disk Au nanopatterns were fabricated on a glass (Figure 2A). SEM images were used to quantify the diameter (99 ± 4 nm) and surface density (∼18 disks/μm^2). Moreover the presence of Au nanodisks on the glass substrate was easily identified by the appearance of a light blue color. After nanodisk fabrication, the Au regions of the surface were chemically modified and used as specific sites for AMY covalent attachment. Polyphenols are known for a strong ability to bind to different surfaces. Therefore, different surface chemistries were screened to minimize PGG background, the 16-mercaptohexadecanoic acid was revealed as an optimal background to chemical modify the Au disk surface (as presented in Table S1, Supporting Information). Subsequently, the thiol terminal carboxyl groups were activated by the carbodiimide activation mechanism. The resulting product experienced nucleophilic substitution by the exposed amine groups of AMY, enabling a covalent coupling to Au

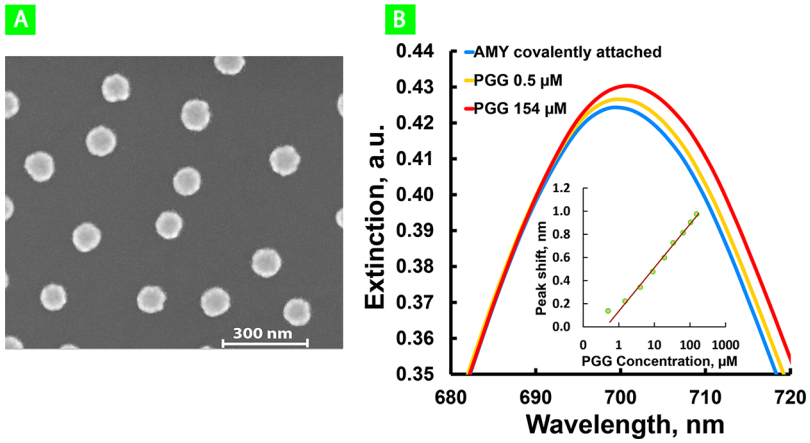

Figure 2. Detection of small molecules with LSPR's (A) scanning electron microscope (SEM) images of the array pattern of Au nanodisks fabricated on a glass substrate, top view. (B) LSPR spectra corresponding to the PGG binding, (inset) the resulting calibration curve for PGG.

disks surface. Although this reaction benefits from the presence of nonprotonated amines, results from surface plasmon resonance (SPR) measurements indicated pH 5 as the optimum pH for AMY immobilization, as shown in Figure S1 (Supporting Information). AMY has a reported isoelectric point f 7.5[54] being slightly positively charged at pH 5, therefore additional electrostatic interaction attract the enzyme to the negative charged surface likely explain the higher binding level response obtained when using pH 5. Unreacted activated groups were blocked with glycine at pH 10.2 (screening of blocking conditions are shown in Figure S2, Supporting Information). The Au disk samples with covalently immobilized AMY were then used to study PGG binding to AMY. The detailed description of the self-assembled monolayer functionalization of the LSPR sensor is presented in the Supporting Information.

The optical spectra of Au nanodisks showed one extinction peak with maximum at ~700 nm in sodium acetate buffer (SA buffer). A representative immobilization of AMY 10 μM induced an average red shift of 0.97 $\pm$ 0.36 nm, indicating a local refractive index increase at the Au nanodisks surface (Figure 2B). The injection of PGG in the flow system resulted in a red shift of the plasmon peak resulting from the contact with AMY covalently attached to Au disks. This interaction was detected for several PGG solutions with concentrations ranging from 0.5 up to 154 μM that promoted a linear shift variation. The detailed modification steps with the corresponding extinction peak shift of LSPR sensors are shown in Figure S3 (Supporting Information). The contact time established between the AMY and PGG was 150 s followed by the exposure of sodium acetate buffer, 5% ethanol (SAE buffer) for another 150 s, (kinetic studies demonstrated that stable binding was established in less than 1 min). Figure 2B displayed the spectra shift corresponding to the lowest PGG concentration, yellow curve, interacting with immobilized AMY, as well as the shift promoted by the highest PGG concentration, represented by the red curve. The interaction with the lowest PGG concentration, 0.5 μM, promoted an average shift of 0.43 $\pm$ 0.09 nm. This red shift indicates that the binding of PGG to AMY is strong with PGG remaining after rinsing.

The PGG binding showed relatively large shifts already at low concentrations compared to changes obtained for further increasing concentrations, suggesting multiple binding sites. For the lowest PGG concentration added, the ratio of PGG/AMY was around 12 and 9 molecules for measurements carried out by SPR and LSPR, respectively. Mapping of the solvent accessible residues in AMY based on the protein structure in the Swiss PDB viewer software indicated 8 patches which have both aromatic and hydrophobic character and 5 patches of purely aromatic character exposed on its surface (Figure S5, Supporting Information). The match to the initial amount of PGG attached at low concentration suggests that these aromatic/hydrophobic patches play an important role at the first contact with PGG. We interpret the first shift as corresponding to the interaction between AMY aromatic/hydrophobic paths and the both aromatic rings and hydroxyl groups of PGG and the later binding at higher concentrations to the complex formation between PGG already bound to the AMY and additional PGG coming to the surface.

The influence of PGG concentration on the LSPR nanosensor response was studied by injecting successive additions of increasing PGG concentrations into the system. Peak shifts to higher wavelength were observed, though relatively small when compared to the shift of the first PGG concentration addition. The shift data presented a linear response with log PGG concentration, indicating concentration dependence. The LSPR λ_{max} shift *versus* log concentration PGG response was measured against the concentration

range from 0.5 to 154.0 μM promoting a total average shift variation from 0.43 to 1.05 nm as can be seen in Figure 1C (inset calibration curve). For the PGG concentration 154 μM the PGG/AMY ratio was ~21 molecules, therefore the aromatic/hydrophobic patches available on its surface are not enough to promote the interaction with PGG suggesting that at higher concentrations either aggregation of PGG with PGG already bound at AMY or binding to other lower affinity surface sites occurred. The affinity between AMY and PGG was in both cases apparently high enough to consider it an irreversible binding. The concentration dependence can then be considered as a rate limiting parameter. In this range of concentrations the sensitivity for PGG was 0.360 $\pm$ 0.02 nm/μM. The standard deviation for all measurements was lower than 5.5% indicating a consistent response from sample to sample and respective calibration.

LSPR Small Molecule Control. We compared the signal observed from PGG interaction to that of a noninteracting small molecule using Dextran 1000 Mw. The experiments were performed in the same way as for PGG where the LSPR sensor was tested for increasing Dextran concentrations ranging from 5 to 10 000 μM. The peak shifts obtained for dextran showed a low or negligible response as shown in Figure 3.

FDTD Simulations. In order to quantitatively understand the experimentally observed spectral shifts we carried out finite-difference time-domain (FDTD) calculations of the optical response of the gold disks. Simulated response for Au nanodisks (100 nm diameter and 20 nm height with 2 nm titanium layer underneath, see Figure S6, Supporting Information) showed peaks resulting from a dipole resonance that matched well to the experimental peaks (see Figure 4). The thiol layer was introduced as a 2 nm thick layer with refractive index of 1.48.[55] The LSPR peak position sensitivity to changes in the bulk refractive index was calculated and compared with that obtained experimentally (matching very well) giving sensitivities of 163 $\pm$ 8 and 161 $\pm$ 1 nm per refractive index unit (RIU), respectively (see Figure S8, Supporting Information). The spatial confinement of the plasmon induced near-field was shown clearly in the field plots (shown in Figure 4C). The highest values of the near-field enhancement of the incoming optical field are localized around the upper and lower rims of the gold disk. The confinement leads to a localization of the sensing region, which can be quantified through FDTD calculations of the nanodisks with an increasing thickness of dielectric layers and gave a characteristic sensing distance of ~17 nm away from their surface, Figure S8 (Supporting Information).

Calculations based on both SPR/LSPR (see Table S2, Supporting Information) and the AMY crystal structure indicate that the AMY formed a dense monolayer.[56] The AMY layer was included in the simulations as a 7 nm layer. The experimental spectrum shift for AMY covalent attachment was 1 nm (see in Figure 4A) with a further shift of 1 nm after exposure to the maximum concentration of PGG in the linear range. FDTD simulations for a 7 nm protein film were matched to the experimental data by tuning the refractive index of the film giving a value of 1.343. In our model the AMY monolayer is closed-packed on the disk surface; however, this low density protein is large when compared to its mass implying high water content on the monolayer. Therefore, the refractive index value of the AMY monolayer results mostly from the large fraction of water. The introduction of PGG was simulated by densification of the 7 nm thick protein layer to model the expected binding at the protein surface, which gives a conservative estimate for the PGG binding. A two layer model with an additional PGG binding layer outside the protein layer would have given larger amounts of PGG bound and higher sensitivities.

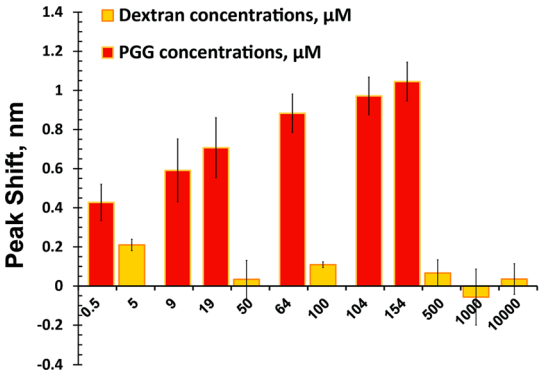

Figure 3. Comparison between AMY interaction with Dextran and PGG as a nonspecific control. Standard errors of means derived from 3 different samples.

LSPR Circular Dichroism Measurements. The binding affinity of polyphenols and salivary proteins, such as AMY, are expected to cause astringency characterized as the sensations of dryness, constriction and puckering of mouth tissues. Therefore, the quantification of PGG/AMY by the LSPR sensor also allows the study of the mechanism of astringency through different stages,[45] first the initial binding to aromatic/hydrophobic patches at low concentration, followed by aggregation/secondary binding sites at the highest concentrations.

Therefore, we utilized circular dichroism (CD) to investigate if AMY conformation is altered by PGG binding, both in bulk solution and bound at surfaces. Typically, biomolecules naturally present CD profiles in the UV (200−300 nm), but these are essentially absent in the visible region.[57]

Conformational changes of AMY promoted by polyphenol compounds in solution determine by CD are already reported. The interaction between AMY and a typical anthocyanin present in food (cyanidin-3-glucoside) lead to a slight decrease of α-helix and increasing trend in β-strand element.[58] Furthermore,

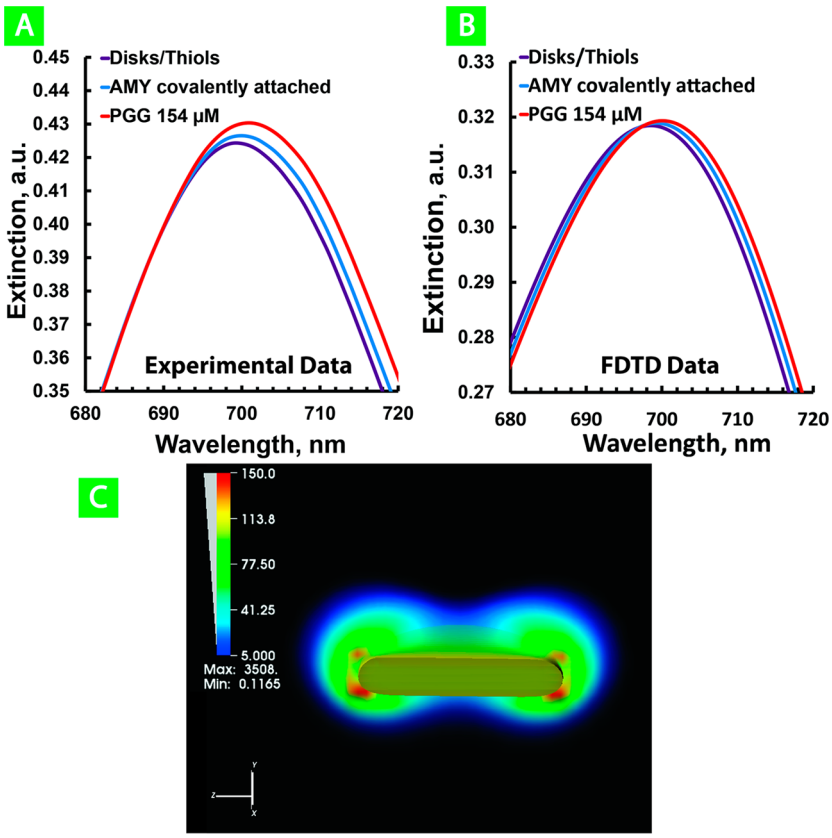

Figure 4. Experimental (A) and FDTD simulated (B) extinction spectra of Disks/thiols, Disks with covalently attached AMY and highest concentration of PGG in the linear range (154 μM). (C) Field enhancement distributions image of the cross section along the center of the nanostructure.

different families of polyphenol have been reported to affect the secondary structure of protein such as human serum albumin and caseins. In general, the α-helical content of the protein decreases upon polyphenols interaction, occasionally a slight increase in the β-sheet structure of the protein was also verified, evidencing that conformational changes are typical from this interaction.[59−61] Here, CD measurements were carried out in solution to study the interaction AMY with PGG in order to confirm any conformational change. The CD spectra in the UV range for AMY in solution with a brown color (Figure 5A), displayed negative ellipticity peak at ∼234 nm that are characteristic of the α-helical secondary structure and derives from n$-\pi^*$ transition. In contrast, CD responses in the visible range are completely absent. The increasing of PGG from 8.9 to 71.4 μM (dark green to purple curve, Figure 5 inset), displayed a wavelength shift associated with an intensity decrease of the α-helical content of the protein promoted by the binding with PGG, as is shown in Figure 5 inset. The spectra were analyzed using CDPro software package including the CONTIN, SELCON and CDSSTR programs combined with a 48-protein reference set[62] to obtain the secondary structural content of the AMY through the binding process. According to the results AMY unmodified control contained 3.2% α-helix, 34.9% β-strand, 17.2% β-turn and 44.1% unordered structure elements. The presence of PGG promoted a slight decrease of α-helix structure from 3.2 to 2.6% accompanied by an increasing trend in β-strand elements from 34.9 to 37.8%, suggesting conformational changes (Table S3, Supporting Information).

The sensitivity of CD is typically low requiring high concentrations of proteins/long experimental runs and precluding measurement of surface bound proteins (except for at high surface area nanoparticles).[63,64] We make use of the strong extinction of our metal nanostructures in the visible wavelength range combined with CD spectroscopy to probe the chiral state of AMY bound at a single monolayer of LSPR sensors and alterations induced by PGG binding. Recent work has highlighted the possibility to probe chirality of dielectric media close to plasmonically active nanostructures demonstrated for biomolecules,[65,66] peptide multilayers[67] or liquid crystals. Here we make use of the effect to detect alterations of conformation of AMY monolayers from binding of PGG. The Au nanodisks were functionalized by the same procedure and conditions as in the LSPR sensor, except for the concentration of AMY immobilized which was 20 μM. For the CD measurements, the glass substrate with Au nanodisks was placed perpendicular to the measurement light beam inside a cuvette filled with buffer.

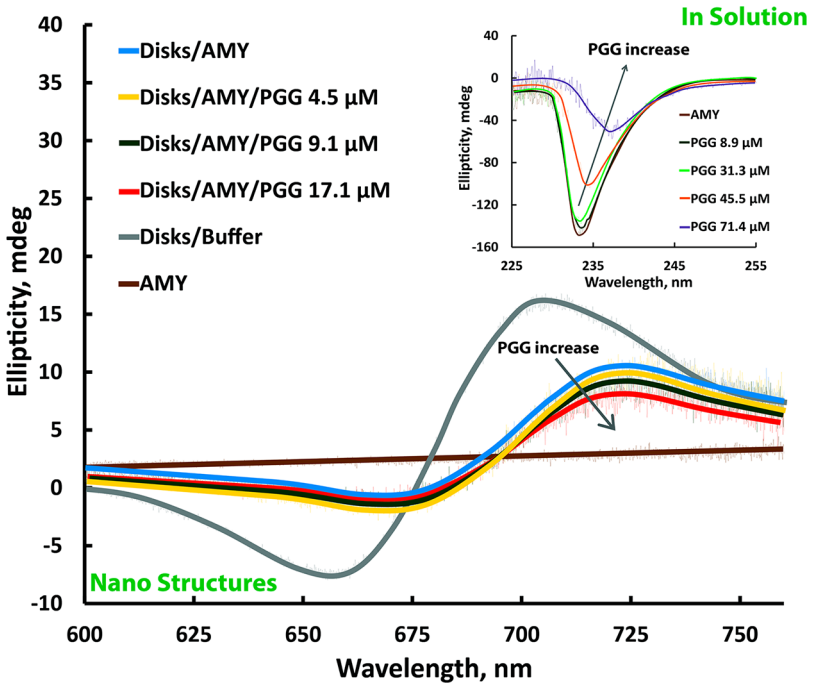

Figure 5. Optical characteristics of nanostructures. Au discs, functionalized with AMY (20 μM), upon PGG binding and AMY without any nanostructure. (Inset) CD measurements in solution, effect of PGG binding on AMY structure.

The Au nanodisks in buffer provided CD responses in the visible range with two peaks, a positive ellipticity peak at ~704 nm and negative ellipticity peak at ~658 nm, corresponding to the gray spectra in Figure 5. The CD spectral feature lies in the same spectral region as the LSPR resonance. The nanostructures although in principle circularly symmetric already presented some chirality, which may be attributed to inhomogeneities of the individual structures (likely differences in the circularity/curvature of the upper and lower disk edges) however symmetric spectra were obtained when flipping the samples 180 deg which indicates that our samples were optically homogeneous.

Although, the Au disks present chirality in the visible spectrum, the assembly of AMY layer introduced a substantially larger red peak shift in the CD responses than that observed in the LSPR characterized in the UV−visible spectra (~13 nm *versus* 1 nm, as shown in both Figure 5 and Figure 2 inset). Simultaneously, the chiral plamonic resonance with the AMY layer also showed a decrease in the peak intensity at both wavelengths 674 and 722 nm, as can be seen by the blue curve in Figure 5. The magnitude of the ellipticity was substantially reduced by the assembled layer which seems to indicate a change in chirality of the dielectric surroundings of the disks.

To verify that the chirality changes were only due to the covalent binding of the protein, the spectrum of AMY in buffer (without nanodisks) was also collected, the nonexistence of CD signals in the visible range was observed by the brown curve of Figure 5. According to our CD measurements performed in solution the AMY presents high β-sheet content (β-34.9%; α-3.2%), as can be seen in Table S3 (Supporting Information). The significant change on the CD spectra by a protein with high β-sheet content was also observed by Hendry's work.[68] They reported that proteins with high β-sheet content induce stronger red shifts on the chiral plasmonic resonances of a chiral metamaterial than high α-helical content proteins, and they correlated decreased β-sheet content to a reduction of the chiral response. Here we show a decrease in chiral response of the Au disks upon PGG interaction correlated to an increased β-sheet content. The interaction of increasing PGG concentrations from 4.5 to 17.1 μM showed a small shift to longer wavelength (~2 nm shift) and a peak intensity reduction. According to the CD performed in solution, PGG interaction with AMY leads to a β-sheet content increment which is consistence with the observed red shift of the chiral plasmonic resonance. Therefore, changes in the conformation of AMY observed in solution seem to be detected on the CD spectra of the chiral nanodisks. CD measurements performed in nanostructures provided qualitative information regarding the structural protein content, though it would be of great interest to obtain a proper quantification which will be future topic of research in our group.

Therefore, it was possible to follow conformation changes by using the same nanostructures used for LSPR sensor, adding extra information about the interaction of AMY and PGG. Here we see chirality of the dielectric surroundings of the disks resulting from

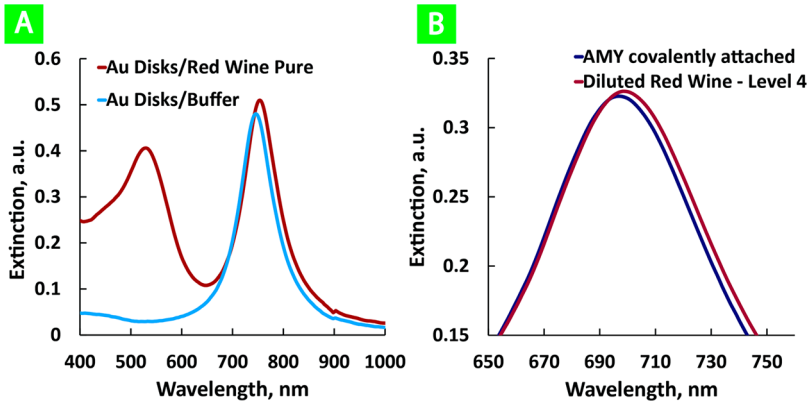

Figure 6. Analysis of wine samples using the LSPR sensor: (A) visible spectra of red wine and buffer; (B) red shift of red wine.

changes in the protein conformation already for levels of PGG where ~12 PGG molecules bind to AMY. These slight conformational changes of AMY, although successfully tracked, were not likely to have significantly influenced the LSPR refractive index readout. FDTD simulations indicated that a massive reduction of film thickness (>80%) with an unphysical refractive index would be required to explain the 1 nm shift of peak position during PGG binding as resulting from altered layer thickness (see Figure S9, Supporting Information).

LSPR Sensor Applied to Real Samples. The obtained results strongly suggest that the interaction of proteins with small molecules taking place at the LSPR sensor may be employed to assess this phenomenon in specific contexts, such as that for protein/polyphenols. Here we tested our sensor in the context of the specific interaction of polyphenols in wine to estimate astringency. This organoleptic sensation is characterized by dryness, roughness and puckering of oral surfaces due to lubrication loss, which results from the interaction of within wine polyphenols and salivary mouth proteins. Although several theories have been proposed for the astringency mechanism the most widely accepted relies on the cross-linking of protein molecules by polyphenols, which act as a polydentate ligand and results in the formation of soluble complexes and/or insoluble precipitates. Analysis of astringency typically focuses in the later stages with formation of insoluble precipitates. The formation of soluble complexes is more difficult to assess and here LSPR sensors seems a suitable tools to estimate this first step of astringency. Wine is a well-known beverage rich in polyphenols however its composition depends on many factors. For example, red wines are rich in polyphenols due to their extraction from grape seeds and skin during the fermentation process or oak contact during aging, while white wines usually shows lower polyphenol content because its production does not involve these stages. Both wine types were tested by estimating the interaction of immobilized AMY on the surface of the sensor and polyphenols from real wine samples (complex matrix). The main drawback of current optical sensors is the color interference of some samples in the detection mode, especially in the visible region. Therefore, both spectra of Au nanodisks in buffer media and a red wine sample were collected and presented in Figure 6A. Comparing the two spectra, it is possible to observe that the plasmonic peak appears ~760 nm, a completely distinct wavelength than the peak resulting from the red color of wine ~540 nm, therefore in the case of red wine analysis, the color will not interfere in the interaction detection between AMY and wine polyphenol. Both spectra in Figure 6A,B correspond to the wine sample with the highest astringency level, the reason that the peak shift in Figure 6B is smaller than that seen in the Figure 6A is only due to wine dilution.

TABLE 1. Polyphenol Concentration Estimation in Terms of PGG Equivalents for Real Wines

wine samples	astringency intensity[a]	peak shift, nm	measured PGG conc, μM	error, %
A	1	0.77 ± 0.14	0.50 ± 0.08	15.4
B	2[b]	0.51 ± 0.2	31.3 ± 6.3	20.1
C	3[b]	1.51 ± 0.30	220 ± 60	27.3
D	4[b]	2.48 ± 0.24	1019 ± 277	27.2

[a] Intensity scale obtained by a sensor panel. [b] Samples diluted hundredfold.

The tested wines had previously been classified by sensorial analysis in terms of astringency through an external entity, ranging in a relative scale from the high (4) to lowest level (1). Two white (Table 1, astringency 1 and 2) and two red wines (Table 1, astringency 3 and 4), with different astringency levels were selected. The immobilization of AMY on nanodisks and the analysis of the real wine samples was monitored by the same procedure and conditions earlier used for pure PGG interaction. All the wine-exposed samples showed a red shift, which is expected from the presence of polyphenols in their composition.

The peak shifts obtained for the wine samples ranged from 0.51 to 2.48 nm, the obtained shifts were used to calculate the polyphenol concentration expressed in PGG equivalents which correlated well with the astringency levels provided by the sensorial panel.

Astringency is associated with the polyphenol content of wine and their capacity to interact with salivary proteins. The large difference in polyphenol content between the red and white wine is expected. The analysis of wine samples also allowed observing if the complexity of the wine matrix would significantly affect the polyphenol reactivity. Astringency levels expressed in PGG equivalent contents were estimated for all wine samples (data shown in Table 1). The white wine samples A and B presented lowest estimated polyphenols concentration than red wine samples C and D. Comparison of the sensorial results and the experimental data, a good correlation was found between the estimated concentration of PGG equivalents in wine samples and their relative astringency level determined by sensorial analysis, furthermore the error of the estimated polyphenol concentration was between 15 and 30% for these detections. At first sight the error may seem large but considering that wine samples are extremely complex and that astringency estimation matches the sensorial analysis, we can state that the LSPR sensor was successfully applied to real samples.

Overall, the estimation of polyphenol concentration and its correlation with astringency levels can be extremely useful as a process control parameter during wine production in order to fit the characteristics of the final product and consequently the consumer's satisfaction. LSPR sensors have the potential to provide rapid and valuable information on astringency in wine as an alternative to time-consuming and expensive sensorial analysis

CONCLUSIONS

Here we utilize plasmonically active gold nanodisks as multifunctional sensors of small molecule–protein interaction. We have demonstrated the quantification of a model molecule (PGG) binding to AMY by using the LSPR peak shift calibrated by FDTD calculations and correlated the level of binding to the protein structure. *In situ* measurement of conformation changes for bound AMY were carried out indirectly *via* plasmonically enhanced CD spectroscopy using gold nanodisks as chiral sensors. The chirality changes of the bound protein layer were correlated to structural alterations of the protein observed upon PGG binding. The potential to carry out both quantification of molecular binding and monitor associated protein structural changes in a sensor format has application in a range of drug discovery and drug mechanistic studies as well as for industrial application in biotechnology and food processing.

METHODS

The fabrication of Au nanodisks on a glass substrate was based on hole mask colloidal lithography,[53] allowing us to create specific spots for AMY immobilization. Images acquired using both scanning electron microscopic (SEM) JEOL Magellan XHR 400 FE-SEM 4 kV spot size ~1 nm and dry atomic force microscopy Bruker Dimension Edge AFM operating in tapping mode were used to characterize the Au nanodisks. The Au nanodisks were modified by self-assembly; the AMY was covalently immobilized on Au nanodisks through amine coupling by EDAC/NHS activation. The extinction spectra of the gold nanostructures on glass substrates and subsequent modifications and interaction of PGG with the AMY were obtained by a commercial UV–vis–NIR spectroscopy (Shimadzu 3600 UV/vis-NIR) with glass substrate as a reference.

CD Spectroscopy was carried out to study AMY-PGG interactions in bulk solution from 225 to 255 nm and immobilized AMY at the Au nanodisks from 600 to 760 nm. CD spectra were collected on a Jasco J-810 spectropolarimeter and using a quartz cuvette with 0.2 cm path length. All simulated data were obtained from finite-difference time-domain (FDTD) calculations performed with the commercial software FDTD Solutions (Lumerical Solutions, Inc., Canada).

All wine samples tested were diluted a hundredfold, except the wine with the lowest level of astringency, sample A.

Conflict of Interest: The authors declare no competing financial interest.

Acknowledgment. The authors acknowledge FCT, Fundação para a Ciência e Tecnologia, for the financial support (SFRH/BD/72479/2010), the FSE, Fundo Social Europeu for the cofinancial support, and CVRVV, Comissão de Viticultura da Região dos Vinhos Verdes, for providing the wine samples and enabling their sensorial analysis.

Supporting Information Available: Materials and methods including Au nanodisks fabrication, self-assembly optimizations and interaction measurements by LSPR, as well as description of data analysis. FDTD calculations of the optical response of the gold disks such as bulk sensitivity, decay lengths and calibration curves for the two-layer model. Atomic force microscopy (AFM) images of bare Au disks and with AMY. Analysis of secondary structural content of the AMY through the binding process by CDPro software package. This material is available free of charge *via* the Internet at http://pubs.acs.org.

REFERENCES AND NOTES

1. Klotz, I. M. Protein Interactions with Small Molecules. *Acc. Chem. Res.* **1974**, *7*, 162–168.
2. Kaushansky, A.; Allen, J. E.; Gordus, A.; Stiffler, M. A.; Karp, E. S.; Chang, B. H.; MacBeath, G. Quantifying Protein–Protein Interactions in High Throughput using Protein Domain Microarrays. *Nat. Protoc.* **2010**, *5*, 773–790.
3. Schreiber, S. L.; Crabtree, G. R. The Mechanism of Action of Cyclosporine-A and FK506. *Immunol. Today* **1992**, *13*, 136–142.
4. Lomenick, B.; Olsen, R. W.; Huang, J. Identification of Direct Protein Targets of Small Molecules. *ACS Chem. Biol.* **2011**, *6*, 34–46.
5. Woods, L. A.; Platt, G. W.; Hellewell, A. L.; Hewitt, E. W.; Homans, S. W.; Ashcroft, A. E.; Radford, S. E. Ligand Binding to Distinct States Diverts Aggregation of an Amyloid-Forming Protein. *Nat. Chem. Biol.* **2011**, *7*, 730–739.
6. Bachovchin, D. A.; Brown, S. J.; Rosen, H.; Cravatt, B. F. Identification of Selective Inhibitors of Uncharacterized Enzymes by High-Throughput Screening with Fluorescent Activity-Based Probes. *Nat. Biotechnol.* **2009**, *27*, 387–394.
7. Collins, I.; Workman, P. New Approaches to Molecular Cancer Therapeutics. *Nat. Chem. Biol.* **2006**, *2*, 689–700.
8. Schenone, M.; Dancik, V.; Wagner, B. K.; Clemons, P. A. Target Identification and Mechanism of Action in Chemical Biology and Drug Discovery. *Nat. Chem. Biol.* **2013**, *9*, 232–240.

9. Zheng, S.; Kim, D.-K.; Park, T. J.; Lee, S. J.; Lee, S. Y. Label-Free Optical Diagnosis of Hepatitis B Virus with Genetically Engineered Fusion Proteins. *Talanta* **2010**, *82*, 803–809.
10. Haes, A. J.; Chang, L.; Klein, W. L.; Van Duyne, R. P. Detection of a Biomarker for Alzheimer's Disease from Synthetic and Clinical Samples using a Nanoscale Optical Biosensor. *J. Am. Chem. Soc.* **2005**, *127*, 2264–2271.
11. Balamurugan, S.; Mayer, K. M.; Lee, S.; Soper, S. A.; Hafner, J. H.; Spivak, D. A. Nanostructure Shape Effects on Response of Plasmonic Aptamer Sensors. *J. Mol. Recognit.* **2013**, *26*, 402–407.
12. Cottat, M.; Thioune, N.; Gabudean, A. M.; Lidgi-Guigui, N.; Focsan, M.; Astilean, S.; de la Chapelle, M. L. Localized Surface Plasmon Resonance (LSPR) Biosensor for the Protein Detection. *Plasmonics* **2013**, *8*, 699–704.
13. Haes, A. J.; Zou, S.; Zhao, J.; Schatz, G. C.; Van Duyne, R. P. Localized Surface Plasmon Resonance Spectroscopy Near Molecular Resonances. *J. Am. Chem. Soc.* **2006**, *128*, 10905–10914.
14. Mazzotta, F.; Wang, G.; Hagglund, C.; Hook, F.; Jonsson, M. P. Nanoplasmonic Biosensing with On-Chip Electrical Detection. *Biosens. Bioelectron.* **2010**, *26*, 1131–1136.
15. Feuz, L.; Jonsson, M. P.; Hook, F. Material-Selective Surface Chemistry for Nanoplasmonic Sensors: Optimizing Sensitivity and Controlling Binding to Local Hot Spots. *Nano Lett.* **2012**, *12*, 873–879.
16. Emani, N. K.; Chung, T. F.; Kildishev, A. V.; Shalaev, V. M.; Chen, Y. P.; Boltasseva, A. Electrical Modulation of Fano Resonance in Plasmonic Nanostructures Using Graphene. *Nano Lett.* **2014**, *14*, 78–82.
17. Fang, Z. Y.; Wang, Y. M.; Schather, A. E.; Liu, Z.; Ajayan, P. M.; de Abajo, F. J. G.; Nordlander, P.; Zhu, X.; Halas, N. J. Active Tunable Absorption Enhancement with Graphene Nanodisk Arrays. *Nano Lett.* **2014**, *14*, 299–304.
18. Zhang, H.; Shih, J.; Zhu, J.; Kotov, N. A. Layered Nanocomposites from Gold Nanoparticles for Neural Prosthetic Devices. *Nano Lett.* **2012**, *12*, 3391–3398.
19. Miller, M. M.; Lazarides, A. A. Sensitivity of Metal Nanoparticle Surface Plasmon Resonance to the Dielectric Environment. *J. Phys. Chem. B* **2005**, *109*, 21556–21565.
20. Willets, K. A.; Van Duyne, R. P. Localized Surface Plasmon Resonance Spectroscopy and Sensing. *Annu. Rev. Phys. Chem.* **2007**, *58*, 267–297.
21. Anker, J. N.; Hall, W. P.; Lyandres, O.; Shah, N. C.; Zhao, J.; Van Duyne, R. P. Biosensing with Plasmonic Nanosensors. *Nat. Mater.* **2008**, *7*, 442–453.
22. Endo, T.; Kerman, K.; Nagatani, N.; Hiepa, H. M.; Kim, D.-K.; Yonezawa, Y.; Nakano, K.; Tamiya, E. Multiple Label-Free Detection of Antigen-Antibody Reaction using Localized Surface Plasmon Resonance-Based Core-Shell Structured Nanoparticle Layer Nanochip. *Anal. Chem.* **2006**, *78*, 6465–6475.
23. Gao, M.; Skolnick, J. A Comprehensive Survey of Small-Molecule Binding Pockets in Proteins. *PLoS Comput. Biol.* **2013**, *9*, 1–12.
24. Greenfield, N. J. Determination of the Folding of Proteins as a Function of Denaturants, Osmolytes or Ligands using Circular Dichroism. *Nat. Protoc.* **2006**, *1*, 2733–2741.
25. Zsila, F.; Bikadi, Z.; Fitos, I.; Simonyi, M. Probing Protein Binding Sites by Circular Dichroism Spectroscopy. *Curr. Drug Discovery Technol.* **2004**, *1*, 133–53.
26. Zsila, F. Circular Dichroism Spectroscopy Is a Sensitive Tool for Investigation of Bilirubin-Enzyme Interactions. *Biomacromolecules* **2011**, *12*, 221–227.
27. Siligardi, G.; Hussain, R.; Patching, S. G.; Phillips-Jones, M. K. Ligand- and Drug-Bindin Studies of Membrane Proteins Revealed through Circular Dichroism Spectroscopy. *Biochim. Biophys. Acta, Biomembr.* **2014**, *1838*, 34–42.
28. Pham, C. L. L.; Kirby, N.; Wood, K.; Ryan, T.; Roberts, B.; Sokolova, A.; Barnham, K. J.; Masters, C. L.; Knott, R. B.; Cappai, R.; *et al.* Guanidine Hydrochloride Denaturation of Dopamine-Induced alpha-Synuclein Oligomers: A Small-Angle X-ray Scattering Study. *Proteins: Struct., Funct., Bioinf.* **2014**, *82*, 10–21.
29. Jin, K. S.; Park, J. K.; Yoon, J.; Rho, Y.; Kim, J. H.; Kim, E. E.; Ree, M. Small-Angle X-ray Scattering Studies on Structures of an Estrogen-related Receptor alpha Ligand Binding Domain and its Complexes with Ligands and Coactivators. *J. Phys. Chem. B* **2008**, *112*, 9603–9612.
30. Lipfert, J.; Doniach, S. Small-Angle X-ray Scattering from RNA, Proteins, and Protein Complexes. *Annu. Rev. Biophys. Biomol. Struct.* **2007**, *36*, 307–327.
31. Cote, M.; Misasi, J.; Ren, T.; Bruchez, A.; Lee, K.; Filone, C. M.; Hensley, L.; Li, Q.; Ory, D.; Chandran, K.; *et al.* Small Molecule Inhibitors Reveal Niemann-Pick C1 is Essential for Ebola Virus Infection. *Nature* **2011**, *477*, 344–348.
32. Srinivasan, P.; Yasgar, A.; Luci, D. K.; Beatty, W. L.; Hu, X.; Andersen, J.; Narum, D. L.; Moch, J. K.; Sun, H.; Haynes, J. D.; *et al.* Disrupting Malaria Parasite AMA1-RON2 Interaction with a Small Molecule Prevents Erythrocyte Invasion. *Nat. Commun.* **2013**, *4*, 1–9.
33. Anand, P.; Sundaram, C.; Jhurani, S.; Kunnumakkara, A. B.; Aggarwal, B. B. Curcumin and Cancer: An "Old-Age" Disease with an "Age-Old" Solution. *Cancer Lett.* **2008**, *267*, 133–164.
34. White, A. W.; Westwell, A. D.; Brahemi, G. Protein-Protein Interactions as Targets for Small-Molecule Therapeutics in Cancer. *Expert Rev. Mol. Med.* **2008**, *10*, 1–14.
35. Selkoe, D. J. Cell Biology of Protein Misfolding: The Examples of Alzheimer's and Parkinson's Diseases. *Nat. Cell Biol.* **2004**, *6*, 1054–1061.
36. Cirillo, D.; Agostini, F.; Klus, P.; Marchese, D.; Rodriguez, S.; Bolognesi, B.; Gaetano Tartaglia, G. Neurodegenerative Diseases: Quantitative Predictions of Protein−RNA Interactions. *RNA* **2013**, *19*, 129–140.
37. Ryan, D. P.; Matthews, J. M. Protein−Protein Interactions in Human Disease. *Curr. Opin. Struct. Biol.* **2005**, *15*, 441–446.
38. Lendel, C.; Bertoncini, C. W.; Cremades, N.; Waudby, C. A.; Vendruscolo, M.; Dobson, C. M.; Schenk, D.; Christodoulou, J.; Toth, G. On the Mechanism of Nonspecific Inhibitors of Protein Aggregation: Dissecting the Interactions of alpha-Synuclein with Congo Red and Lacmoid. *Biochemistry* **2009**, *48*, 8322–8334.
39. Porat, Y.; Abramowitz, A.; Gazit, E. Inhibition of Amyloid Fibril Formation by Polyphenols: Structural Similarity and Aromatic Interactions as a Common Inhibition Mechanism. *Chem. Biol. Drug Des.* **2006**, *67*, 27–37.
40. Di Pietrantonio, F.; Cannata, D.; Benetti, M.; Verona, E.; Varriale, A.; Staiano, M.; D'Auria, S. Detection of Odorant Molecules *via* Surface Acoustic Wave Biosensor Array based on Odorant-Binding Proteins. *Biosens. Bioelectron.* **2013**, *41*, 328–334.
41. Ai, K. L.; Liu, Y. L.; Lu, L. H. Hydrogen-Bonding Recognition-Induced Color Change of Gold Nanoparticles for Visual Detection of Melamine in Raw Milk and Infant Formula. *J. Am. Chem. Soc.* **2009**, *131*, 9496–9497.
42. Peng, B.; Li, G.; Li, D.; Dodson, S.; Zhang, Q.; Zhang, J.; Lee, Y. H.; Demir, H. V.; Ling, X. Y.; Xiong, Q. Vertically Aligned Gold Nanorod Monolayer on Arbitrary Substrates: Self-Assembly and Femtomolar Detection of Food Contaminants. *ACS Nano* **2013**, *7*, 5993–6000.
43. Ryder, A. G. Surface Enhanced Raman Scattering for Narcotic Detection and Applications to Chemical Biology. *Curr. Opin. Chem. Biol.* **2005**, *9*, 489–493.
44. Han, X. X.; Zhao, B.; Ozaki, Y. Label-Free Detection in Biological Applications of Surface-Enhanced Raman Scattering. *TrAC, Trends Anal. Chem.* **2012**, *38*, 67–78.
45. de Freitas, V.; Mateus, N. Protein/Polyphenol Interactions: Past and Present Contributions. Mechanisms of Astringency Perception. *Curr. Org. Chem.* **2012**, *16*, 724–746.
46. Lenlerpetersen, P.; Grove, A.; Brock, A. alpha-Amylase in Resectable Lung-Cancer. *Eur. Respir. J.* **1994**, *7*, 941–945.
47. Chiappelli, F.; Iribarren, F. J.; Prolo, P. Salivary Biomarkers in Psychobiological Medicine. *Bioinformation* **2006**, *1*, 331–334.
48. Cozzone, P.; Pasero, L.; Marchism, G. Characterization of Porcine Pancreatic Isoamylases—Separation and Amino Acid Composition. *Biochim. Biophys. Acta* **1970**, *200*, 590–593.
49. Larson, S. B.; Day, J. S.; McPherson, A. X-ray Crystallographic Analyses of Pig Pancreatic alpha-Amylase with

Limit Dextrin, Oligosaccharide, and alpha-Cyclodextrin. *Biochemistry* **2010**, *49*, 3101–3115.
50. Gyemant, G.; Zajacz, A.; Becsi, B.; Ragunath, C.; Ramasubbu, N.; Erdodi, F.; Batta, G.; Kandra, L. Evidence for Pentagalloyl Glucose Binding to Human Salivary alpha-Amylase through Aromatic Amino Acid Residues. *Biochim. Biophys. Acta, Proteins Proteomics* **2009**, *1794*, 291–296.
51. de Moura, C. F. G.; Noguti, J.; de Jesus, G. P. P.; Ribeiro, F. A. P.; Garcia, F. A.; Gollucke, A. P. B.; Aguiar, O.; Ribeiro, D. A. Polyphenols as a Chemopreventive Agent in Oral Carcinogenesis: Putative Mechanisms of Action using *In-Vitro* and *In-Vivo* Test Systems. *Eur. J. Cancer Prev.* **2013**, *22*, 467–472.
52. McRae, J. M.; Kennedy, J. A. Wine and Grape Tannin Interactions with Salivary Proteins and their Impact on Astringency: A Review of Current Research. *Molecules* **2011**, *16*, 2348–2364.
53. Fredriksson, H.; Alaverdyan, Y.; Dmitriev, A.; Langhammer, C.; Sutherland, D. S.; Zaech, M.; Kasemo, B. Hole-Mask Colloidal Lithography. *Adv. Mater.* **2007**, *19*, 4297–4302.
54. Ajandouz, E. H.; Marchismouren, G. J. Subsite Mapping of Porcine Pancreatic alpha-Amylase I and alpha-Amylase II using 4-Nitrophenyl-alpha-Maltooligosaccharides. *Carbohydr. Res.* **1995**, *268*, 267–277.
55. Hinterwirth, H.; Kappel, S.; Waitz, T.; Prohaska, T.; Lindner, W.; Lammerhofer, M. Quantifying Thiol Ligand Density of Self-Assembled Monolayers on Gold Nanoparticles by Inductively Coupled Plasma-Mass Spectrometry. *ACS Nano* **2013**, *7*, 1129–1136.
56. Hinrichsen, E. L.; Feder, J.; Jossang, T. Geometry of Random Sequential Adsorption. *J. Stat. Phys.* **1986**, *44*, 793–827.
57. Berova, N.; Nakanishi, K.; Woody, R. W. *Circular Dichroism: Principles and Applications*; Wiley-VCH: New York, 2000.
58. Wiese, S.; Gaertner, S.; Rawel, H. M.; Winterhalter, P.; Kulling, S. E. Protein Interactions with Cyanidin-3-Glucoside and its Influence on alpha-Amylase Activity. *J. Sci. Food Agric.* **2009**, *89*, 33–40.
59. Bian, Q. Q.; Liu, J. Q.; Tian, J. N.; Hu, Z. D. Binding of Genistein to Human Serum Albumin Demonstrated using Tryptophan Fluorescence Quenching. *Int. J. Biol. Macromol.* **2004**, *34*, 333–337.
60. Maiti, T. K.; Ghosh, K. S.; Dasgupta, S. Interaction of (−)-Epigallocatechin-3-Gallate with Human Serum Albumin: Fluorescence, Fourier Transform Infrared, Circular Dichroism, and Docking Studies. *Proteins: Struct., Funct., Bioinf.* **2006**, *64*, 355–362.
61. Hasni, I.; Bourassa, P.; Hamdani, S.; Samson, G.; Carpentier, R.; Tajmir-Riahi, H.-A. Interaction of Milk alpha- and beta-Caseins with Tea Polyphenols. *Food Chem.* **2011**, *126*, 630–639.
62. Sreerama, N.; Venyaminov, S. Y.; Woody, R. W. Estimation of Protein Secondary Structure from Circular Dichroism Spectra: Inclusion of Denatured Proteins with Native Proteins in the Analysis. *Anal. Biochem.* **2000**, *287*, 243–251.
63. Wang, J.; Jensen, U. B.; Jensen, G. V.; Shipovskov, S.; Balakrishnan, V. S.; Otzen, D.; Pedersen, J. S.; Besenbacher, F.; Sutherland, D. S. Soft Interactions at Nanoparticles Alter Protein Function and Conformation in a Size Dependent Manner. *Nano Lett.* **2011**, *11*, 4985–4991.
64. Jiang, X.; Jiang, U. G.; Jin, Y. D.; Wang, E. K.; Dong, S. J. Effect of Colloidal Gold Size on the Conformational Changes of Adsorbed Cytochrome C: Probing by Circular Dichroism, UV−Visible, and Infrared Spectroscopy. *Biomacromolecules* **2005**, *6*, 46–53.
65. Abdulrahman, N. A.; Fan, Z.; Tonooka, T.; Kelly, S. M.; Gadegaard, N.; Hendry, E.; Govorov, A. O.; Kadodwala, M. Induced Chirality through Electromagnetic Coupling between Chiral Molecular Layers and Plasmonic Nanostructures. *Nano Lett.* **2012**, *12*, 977–983.
66. Wu, X.; Xu, L.; Liu, L.; Ma, W.; Yin, H.; Kuang, H.; Wang, L.; Xu, C.; Kotov, N. A. Unexpected Chirality of Nanoparticle Dimers and Ultrasensitive Chiroplasmonic Bioanalysis. *J. Am. Chem. Soc.* **2013**, *135*, 18629–18636.
67. Slocik, J. M.; Govorov, A. O.; Naik, R. R. Plasmonic Circular Dichroism of Peptide-Functionalized Gold Nanoparticles. *Nano Lett.* **2011**, *11*, 701–705.
68. Hendry, E.; Carpy, T.; Johnston, J.; Popland, M.; Mikhaylovskiy, R. V.; Lapthorn, A. J.; Kelly, S. M.; Barron, L. D.; Gadegaard, N.; Kadodwala, M. Ultrasensitive Detection and Characterization of Biomolecules using Superchiral Fields. *Nat. Nanotechnol.* **2010**, *5*, 783–787.